Supporting Information

Shedding light on the mechanism of asymmetric track etching: an interplay between latent track structure, etchant diffusion and osmotic flow

Pavel Y. Apel,[a,b] Valery V. Bashevoy,[a] Irina V. Blonskaya,[a] Nikolay E. Lizunov,[a] Oleg L. Orelovitch[a] and Christina Trautmann[c,d]

[a] *Joint Institute for Nuclear Research, Joliot-Curie street 6, 141980 Dubna, Russian Federation; E-mail: apel@jinr.ru*
[b] *Dubna State University, Universitetskaya street 19, 141980 Dubna, Russian Federation*
[c] *GSI Helmholtzzentrum fűr Schwerionenforschung, Planckstraße 1, 64291 Darmstadt, Germany*
[d] *Materialwissenschaft, Technische Universität Darmstadt, Alarich-Weiss-Straße 2, 64287 Darmstadt Germany*

1. Effect of stopping solutions on the breakthrough time and track etching rate

Asymmetric etching of a large number of single-track samples was performed in order to measure breakthrough times under different etching conditions. One compartment of a two-compartment electrochemical cell was filled with 9 M NaOH and the other with a stopping solution (as described in Ref. [1]). For the stopping solution composed of 2 M KCl and 2 M HCOOH (50:50, v/v), a typical conductance vs. etching time curve is presented in the main text of the manuscript (Fig. 3). In some experiments, solutions of single reagents (1M KCl or 1M HCOOH) were employed as stopping solutions. Conductometric monitoring of the etching process was performed in AC mode with a PC-controlled LCR-meter (HiTESTER 3522-50, HIOKI E. E. Corporation, Japan).

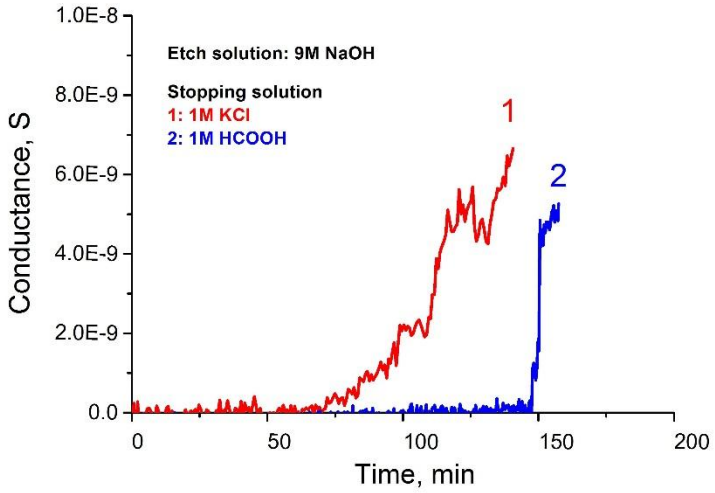

Fig. 1S. Conductometric etching of two foils containing a single Au ion track each. PET foil 12 μm thick. Etchant: 9M NaOH. Stopping solution: aqueous 1M KCl (curve 1) and 1M HCOOH (curve 2). The electrical conductance through the cell was measured in AC mode at a voltage of 0.5 V. Temperature 22°C.

Two typical conductance vs. etching time curves are shown in Fig. 1S. With 1M KCl as the stopping solution, a detectable increase in current above background was observed at ~ 72 min (curve 1). Further increases of the pore conductance are typically slow and irregular. In the case of the acidic stopping solution (1M HCOOH, curve 2), the breakthrough time t_b was approximately 145 min.

The track etching rate V_T is calculated using the following formula:

$$V_T = L_o / t_b$$

where L_o is the initial thickness of the foil (equal to 12 μm). Therefore, for the two experiments illustrated in Fig. 1S we obtained respective V_T values of 167 and 83 nm/min. The higher value corresponds to the neutral stopping solution (1M KCl).

The track to bulk etching rate ratio, V_T / V_B, is ~83 and ~41 for these stopping solutions (1M KCl and 1M HCOOH, respectively). The calculated double cone angles are 1.4 and 2.8°, respectively. Note that in reality the pore channels at the moment of breakthrough are trumpet-like and, therefore, the wide part of the pore has a slightly larger cone angle than the narrowing towards the tip part.

2. FESEM observation of pores etched using different stopping solutions and determination of cone angle

Multi-track samples were etched in a cell adopted for osmotic flow measurements. After observation of osmotic flux and completing the etching, the samples were rinsed, dried, embrittled using intensive UV exposure and prepared for FESEM observation. Fractured samples were coated with a thin (10 nm) layer of chromium and examined using a Hitachi SU8020 FESEM instrument. Pore channels cleaved along their axes were chosen for imaging. Typical images are presented in Fig. 2S. The pore channels consist of long conical parts and rounded or bullet- or acorn-like tips. The conical parts of the channels were used to estimate the double cone angle 2α.

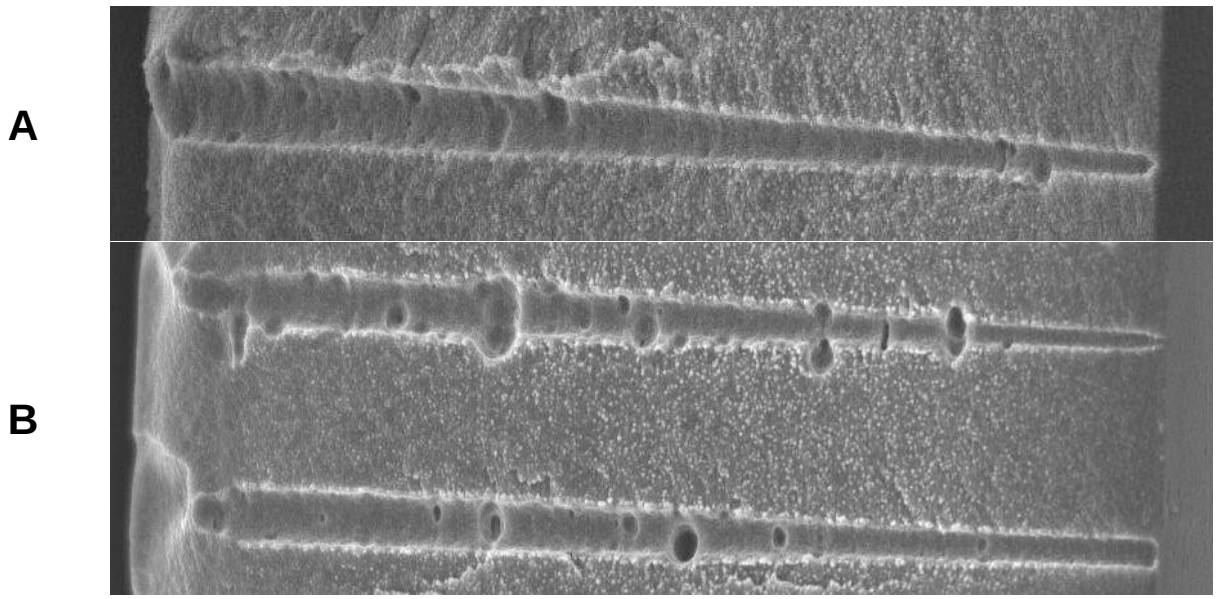

Fig. 2S. Representative FESEM images of longitudinal profiles of pores etched for 50-60 min after breakthrough. The pores were fabricated using asymmetric etching with different stopping solutions: 2M KCl+2M HCOOH, 50:50 (A), and 1 M KCl (B). Etchant: 9M NaOH. Temperature: 22°C. The cavities along the channels are ascribed to the inhomogeneity of the PET matrix material.

The estimated cone angles 2α for the pores of Fig. 2S are 3.8° (A), 2.5° and 2.0° (B), with an uncertainty of approximately ± 0.3°.

Thus, the data derived from Figures 1S and 2S show that presence of formic acid in the stopping solution leads to a decrease in the etching rate along the track and, concomitantly, an increase in the cone angle. This is a direct consequence of the recently reported effect of pH on the ionic permeability of latent tracks [2].

3. Morphology and composition of precipitate nanocrystals formed at the pore tips

FESEM examination of the samples subjected to longtime (200-300 min) asymmetric etching, made it possible to observe the accumulation of a nanocrystalline precipitate on the pore-bearing foil surface in contact with the alkali solution during etching. With increasing time of etching, the particles of the precipitate obviously undergo a transformation from platelets (see Fig. 9(A) and 10(A) in the main manuscript) to "desert-rose" or "flower-like" shapes. Fig. 3S(A) shows a fractured foil sample on the upper surface of which both platelet-shaped (circled) and flower-shaped crystals are seen. Fig. 3S(B) shows crystals of well-pronounced flower-like shape; each crystal corresponds to a pore.

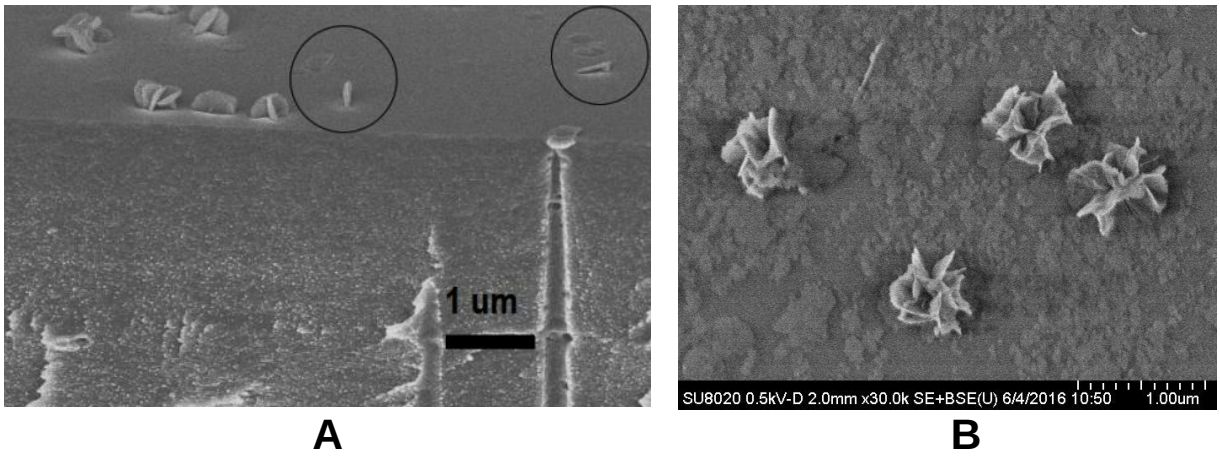

Fig. 3S. Fracture (A) and surface (B) of ion-track foil samples subjected to asymmetric etching. Etchant: 9M NaOH. Stopping solution: 1M KCl. The side that was in contact with the stopping solution is shown.

Energy-dispersive X-ray element analysis of the nanoparticles on the sample surfaces was carried out with a Thermo Scientific™ NORAN™ System 7. Fig. 4S shows the spectra obtained when the electron beam was directed onto the sample surface area free of any particles (A), a flower-like crystal (B), and on a platelet on the surface (C). The surface of the sample contains measurable quantities of C, O, Cr, Al and Si (spectrum A). Carbon and oxygen belong to the polymer (PET). Chromium, used for coating, is also detected as a peak that overlaps with the oxygen peak. The sample holder causes the appearance of aluminum and silicon spectral lines. The spectrum obtained from a flower-like crystal (spectrum B) contains peaks of all elements mentioned above and a well-pronounced peak of magnesium. The signal obtained from a platelet on the sample surface (spectrum C) has a lower, but yet significant, contribution from magnesium.

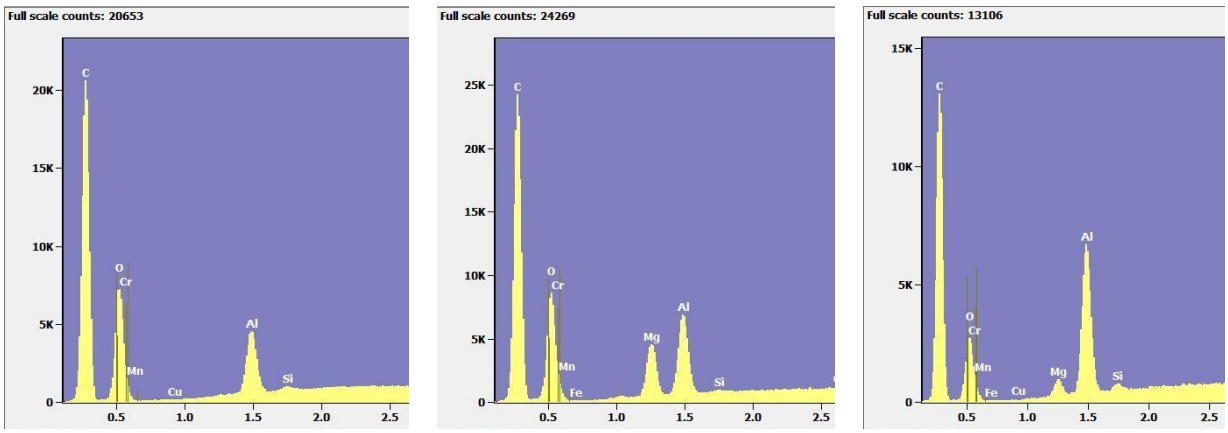

Fig. 4S. Energy dispersive X-ray spectra of a clean sample surface (A), a flower-like crystal (B) and a platelet (C). Number of counts and photon energy (in keV) are shown along the vertical and horizontal axes, respectively. The surface of a sample in contact with a 1M KCl stopping solution during asymmetric etching was analyzed. The chromium signal originates from a sputter layer applied before FESEM examination.

4. Error analysis

4.1. Tip radius in the "conical" approximation

The tip radius r_c of a single pore in the "conical" approximation is calculated using the well-known formula [1]:

$$G_D = \frac{k\pi r_c R}{L} \qquad (1)$$

Here R is the cone base radius, k is the specific conductivity, L is the foil thickness and G_D is the conductance of the solution in the pore measured at the point in time when the second etching stage is commencing (i.e. when step II starts). These quantities are experimentally determined factors which contribute to the uncertainty in the determination of r_c. The contributions from errors in the measurements of the sample thickness, of the order of ± 3 %, and of the specific conductivity of the solution (± 1 %) are relatively small. The cone base radius R of single pore samples cannot be measured directly with SEM examinations because it is physically impossible to locate a single pore of micrometer (or even less) dimensions in a macroscopic sample. Therefore a statistically determined mean cone base radius R and a standard deviation for R are determined from SEM examinations of a large number of pores on multiple pore samples, etched in the conductometric cell under identical conditions as the single pore sample whose tip radius we must estimate through formula (1). Typical micrographs are shown in Fig. 5S. In experiments of this kind the pore openings are generally elliptical in shape [3]. To find a representative value of the mean pore radius R and its standard deviation, the small and large axes of each pore opening were measured and a geometrical mean was calculated from these two quantities for every individual pore and divided by a factor of 2. The variation of the pore base radius within one image obtained in this way is typically very small. However, analysis of several micrographs taken from different sample areas leads to a widening of the variation. The standard deviation of R values found in this way for images taken over extensive sample areas, reaches 5%. This is due to variations in the polymer etching behavior over different areas on a sample. Since the etching behavior of the sample area where a single pore is located is unknown, we must use the sample standard deviation in order to characterize the resulting random error. The conductance measurements in the high impedance range are characterized by a calibration uncertainty of 9%.

Combining the independent uncertainties associated with the above factors in quadrature, we obtain the resulting error of ~11 %.

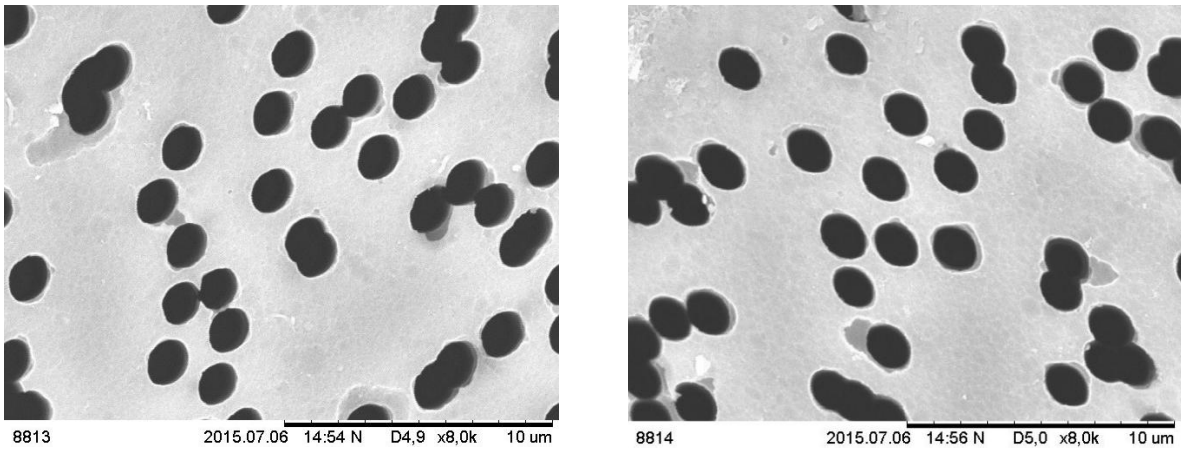

Fig. 5S. SEM images of ion-irradiated PET foil subjected to asymmetric etching. The side treated with 9M NaOH for two samples etched in parallel under identical conditions is shown.

4.2. Tip radius in the "trumpet" approximation

The tip radius r in the "trumpet" pore shape approximation is calculated by the following formula:

$$r(t) = (1+V_B/V_T)^{-1/2}\left[\frac{(1-V_B/V_T)}{R^2(t)} - \left(\frac{k\pi}{V_T}\right)\frac{d}{dt}\,1/G(t)\right]^{-1/2} \qquad (2)$$

Using equation (2), the tip radius as a function of time, $r(t)$, was calculated from the values we measured for $R(t)$, $G(t)$, V_T, V_B, and k. The pore base radius $R(t)$ as a function of time was determined by SEM examination of multi-pore samples as described in Ref. [3]. The value of $r(t)$ determined in the beginning of etching step II (at the moment t_{abs} = 0) corresponds to the tip radius r_t.

Because V_T is significantly larger than V_B in the samples used in this work, the quantities (1 + V_B/V_T) and (1 - V_B/V_T) are very close to 1 and, therefore, random uncertainties in the determination of V_B and V_T practically do not contribute to the error in the determination of r_t. The two terms in the square brackets differ drastically in their contributions to the uncertainty in the determination of the tip radius. At short times t_{abs}, the first term is typically 3 orders of magnitude smaller than the second one. This means that the error in the base radius R does not significantly affect the values of tip radii calculated in this way. Therefore, only uncertainties associated with k, V_T and $1/G$ should be considered. The first two factors cause errors of ± 1 %, and ± 3 %, respectively. The electrical measurements make the most considerable contribution. The error associated with the differentiation of the $1/G(t)$ function depends on the level of electrical noise and the time increment between measurements. In most of our experiments the time increment was chosen equal to 30 s. Taking into account the calibration error, we estimate the resulting uncertainty in $d[1/G(t)]/dt$ as ≤ 15 %. Summing the independent uncertainties in quadrature, we obtain an error of ~15.3% for the expression in the square brackets and finally an error of ~ 8 % for the tip radius r_t calculated in the "trumpet" approximation.

Note that with increasing etching time t_{abs} the relative contributions of the two terms in the square brackets in eq. (2) rapidly change. The first term, $(1 - V_B/V_T)/R(t)$, plays a significant role for the accurate determination of the whole pore profile shown in Fig. 4 in the main text. However, it is practically insignificant for the determination of the pore tip radius.

References

1. P. Yu. Apel, Yu. E. Korchev, Z. Siwy, R. Spohr and M. Yoshida, *Nucl. Instrum. Methods Phys. Res. B*, 2001, 184, 337.

2. Q. Wen, D. Yan, M. Wang, Y. Ling, P. Wang, P. Kluth, D. Schauris, C. Trautmann, P. Apel, W. Guo, G. Xiao, J. Liu, J. Xue, and Y. Wang., *Adv. Func. Mater*., 2016, DOI: 10.1002/adfm.201601689.

3. P. Yu. Apel, I. V. Blonskaya, O. L. Orelovitch, B. A. Sartowska and R. Spohr, *Nanotechnology*, 2012, 23, 225503.